Mineralogical Magazine (2024), **88**, 244–254
doi:10.1180/mgm.2024.11

CAMBRIDGE UNIVERSITY PRESS

Article

The crystal structure of charmarite – the first case of a 11 × 11 Å superstructure mesh in layered double hydroxides

Elena S. Zhitova[1], Andrey A. Zolotarev[1,2], Anatoly V. Kasatkin[3], Rezeda M. Sheveleva[1,2], Sergey V. Krivovichev[2,4], Igor V. Pekov[5] and Vladimir N. Bocharov[2]

[1]Institute of Volcanology and Seismology, Russian Academy of Sciences, Bulvar Piipa 9, 683006 Petropavlovsk-Kamchatsky, Russia; [2]St. Petersburg State University, University Emb. 7/9, 199034 St. Petersburg, Russia; [3]Fersman Mineralogical Museum, Russian Academy of Science, Leninskiy Prospect 18-2, 119071 Moscow, Russia; [4]Nanomaterials Research Centre, Kola Science Centre, Russian Academy of Sciences, Fersman Street 14, 184209 Apatity, Russia; and [5]Faculty of Geology, Moscow State University, Leninskie Gory 1, 119991 Moscow, Russia

Abstract

Charmarite, $Mn_4Al_2(OH)_{12}CO_3{\cdot}3H_2O$, is a hydrotalcite supergroup member (or layered double hydroxide, LDH) with a previously unknown crystal structure and a Mn^{2+}-analogue of quintinite (commonly erroneously reported as '2:1 hydrotalcite'). The single-crystal X-ray diffraction (XRD) data were obtained from the specimen from Mont Saint-Hilaire, Québec, Canada and are best processed in the space group $P\bar{3}$, $a = 10.9630(4)$, $c = 15.0732(5)$ Å and $V = 1568.89(12)$ Å^3. The crystal structure has been solved by direct methods and refined to $R_1 = 0.0750$ for 3801 unique reflections with $F_o > 2\sigma(F_o)$. The charmarite structure has long-range periodicity in the *xy* plane due to $2\sqrt{3}a' \times 2\sqrt{3}a'$ scheme (or 11 × 11 Å) determined for LDHs for the first time (where a' is a subcell parameter ≈ 3.2 Å). This periodicity is produced by the combination of two superstructures formed by: (1) Mn^{2+} and Al^{3+} ordering in the metal-hydroxide layers $[Mn_4Al_2(OH)_{12}]^{2+}$ according to the $\sqrt{3}a' \times \sqrt{3}a'$ pattern and (2) the $(CO_3)^{2-}$ ordering according to the $2a' \times 2a'$ pattern in the $[CO_3(H_2O)_3]^{2-}$ interlayer sheet in order to avoid close contacts between adjacent carbonate groups. The $2\sqrt{3}a' \times 2\sqrt{3}a'$ superstructure is an example of the adaptability of the components of the interlayer space to the charge distribution of the metal-hydroxyl layers. The Mn^{2+} and Al^{3+} cations have a large difference in size, which apparently leads to the considerable degree of their order as di- and trivalent cations resulting in a higher degree of statistical order of the interlayer components. Both powder and single-crystal XRD data show that the samples studied belong to the hexagonal branch of two-layer polytypes (2*T* or 2*H*) with $d_{00n} \approx 7.57$ Å. The chemical composition of the samples studied is close to the ideal formula. The Raman spectrum of charmarite is reported and the band assignment is provided.

Keywords: charmarite; quintinite; hydrotalcite; layered double hydroxide; natural LDH; crystal structure; Mont Saint-Hilaire alkaline complex

(Received 1 November 2023; accepted 16 February 2024; Accepted Manuscript published online: 8 March 2024; Associate Editor: G. Diego Gatta)

Introduction

Charmarite, ideally $Mn_4Al_2(OH)_{12}CO_3{\cdot}3H_2O$, is a member of the quintinite group (with the ratio between di- and trivalent cations equal to M^{2+}:M^{3+} = 2:1), which is a part of the hydrotalcite supergroup (Mills *et al.*, 2012), a natural branch of the layered double hydroxide (LDH) family (Rives, 2001; Evans and Slade, 2005). Layered double hydroxides are united by a common structural motif in which brucite-like metal-hydroxyl layers (or octahedral sheets) formed by di- and trivalent (in specific cases also monovalent) metals and interlayers alternate (Rives, 2001). The positive charge of the brucite-like metal-hydroxide layers is compensated by the negatively charged interlayer species. In some cases, metal-hydroxide layers are gibbsite-based (formed primarily by trivalent cations), where monovalent cations [or divalent cations as shown by synthetic materials (Andersen *et al.*, 2021)] produce the positive charge of the layers (Serna *et al.*, 1982; Sissoko *et al.*, 1985; Britto and Kamath, 2011; Karpenko *et al.*, 2020). Layered double hydroxides are used in catalytic (Karim *et al.*, 2022; Xu and Wei, 2018; Bosa *et al.*, 2023) and pharmaceutical (Guilherme *et al.*, 2022) applications, are of interest from the material science point of view as sorbents and ion exchangers (Forano *et al.*, 2006), and are useful for the design of new materials (Sotiles and Wypych, 2019). The synthetic analogue of charmarite can be obtained by co-precipitation and may be of interest for catalytic applications (Grand *et al.*, 2010).

Charmarite was first described in well-shaped hexagonal crystals from the Mont Saint-Hilaire alkaline complex, Québec, Canada in two polytypic modifications, 2*H* and 3*T* (Chao and Gault, 1997). In the cited paper, charmarite was described together with two other new minerals that have the same stoichiometry: its Mg-analogue quintinite, $Mg_4Al_2(OH)_{12}CO_3{\cdot}3H_2O$, and its Fe^{2+}-analogue caresite, $Fe^{2+}_4Al_2(OH)_{12}CO_3{\cdot}3H_2O$. The work by Chao and Gault (1997) turned out to be pioneering in the approach to quintinite (and, consequently, quintinite-group minerals), which has been finally separated from hydrotalcite after

Corresponding author: Elena Zhitova; Email: zhitova_es@mail.ru
Cite this article: Zhitova E.S., Zolotarev A.A., Kasatkin A.V., Sheveleva R.M., Krivovichev S.V., Pekov I.V. and Bocharov V.N. (2024) The crystal structure of charmarite – the first case of a 11 × 11 Å superstructure mesh in layered double hydroxides. *Mineralogical Magazine* **88**, 244–254. https://doi.org/10.1180/mgm.2024.11

Table 1. Unit-cell parameters of quintinite-group minerals: charmarite, caresite and quintinite.

Mineral Formula	Charmarite	Charmarite	Quintinite $M^{2+}_4Al^{3+}_2(OH)_{12}CO_3{\cdot}3H_2O$	Quintinite	Caresite
M^{2+}	Mn	Mn	Mg	Mg	Fe
Polytype	2*H*	3*T*	2*H*	3*T*	3*T*
Space group	$P6_322$	$P3_112$ or $P3_212$	$P6_322$	$P3_112$ or $P3_212$	$P3_112$ or $P3_212$
a (Å)	10.985(3)	10.985(3)	10.571(1)	10.558(2)	10.805(3)
c (Å)	15.10(2)	22.63(3)	15.1139(7)	22.71(3)	22.48(3)
V (Å^3)	1578(3)	2366(4)	1465(1)	2192(3)	2273(4)
Z	4	6	4	6	6
a' (Å) [(1)]	3.17	3.17	3.05	3.05	3.12
d_{00n} (Å) [(2)]	7.55 (×2)	7.54 (×3)	7.57 (×2)	7.57 (×3)	7.49 (×3)
Reference			Chao and Gault (1997)		
Mineral			Quintinite		
Polytype	3*R*	1*M*	2*H*	2*T*	2*T*–3*c*
Space group	$R\bar{3}m$	*C*2/*m*	$P6_3/mmc$	$P\bar{3}c1$	*R*32
a (Å)	3.06	5.23–5.29	3.02–3.06	5.25–5.31	5.27
b (Å)	= *a*	9.05–9.15	= *a*	= *a*	= *a*
c (Å)	22.67	7.70–7.81	15.06–15.23	15.07–15.23	45.36
β (°)	90	103.0–103.2	90	90	90
V (Å^3)	184.2	356–367	120–124	360–371	1093.0
a' (Å)	3.06	3.02–3.06	3.02–3.06	3.03–3.07	3.05
d_{00n} (Å)	7.56	7.53–7.61	7.56–7.63	7.53–7.61	7.56
References	Zhitova *et al.* (2018)	Krivovichev *et al.* (2010b, 2012); Zhitova *et al.* (2017)	Zhitova *et al.* (2010)	Zhitova *et al.* (2018)	Krivovichev *et al.* (2010a)

[(1)] *a'* is the distance between two neighbouring *M* cations;
[(2)] d_{00n} is the distance between two neighbouring octahedral sheets.

155 years, during which time two phases of different stoichiometry and properties where under the common name 'hydrotalcite'. Later studies showed a wider distribution of quintinite compared to hydrotalcite and fundamental structural differences between the two minerals, especially with respect to the layer charge densities and associated properties (Wang *et al.*, 2009; Mills *et al.*, 2016; Zhitova *et al.*, 2016, 2018).

Crystal structures of most LDHs remain unknown, owing to the absence of single crystals for synthetic materials and, as a result, the absence of starting crystal-structure models for the refinement of powder X-ray diffraction data. In contrast, a number of structure models for synthetic LDHs have been studied based on investigations of their natural analogues (see summary in Mills *et al.*, 2012 and Zhitova *et al.*, 2019a).

To date, charmarite is an endemic mineral with an unknown crystal structure. Charmarite is closely related to quintinite and caresite in terms of stoichiometry and, in general, chemistry. This prompts us to discuss these minerals together. In the work of Chao and Gault (1997) the unit-cell parameters of quintinite, caresite and charmarite have been determined by single-crystal photographic methods and refined by least-squares methods using powder XRD data (Table 1). Based on the single-crystal X-ray photographs Chao and Gault (1997) suggested the presence of a $2\sqrt{3}a' \times 2\sqrt{3}a'$ (or $\sqrt{12}a' \times \sqrt{12}a'$) superstructure in all three minerals interpreted as ordering of di- and trivalent cations (Mills *et al.*, 2012). The first crystal structure determination of quintinite (Arakcheeva *et al.*, 1996) proposed the presence of only the $\sqrt{3}a' \times \sqrt{3}a'$ superstructure (*a'* is not listed further in designation of superstructures) due to the ordered arrangement of di- and trivalent cations. Systematic studies of crystal structures of quintinite from different worldwide localities indicated the existence of at least five polytypes differing by the presence or absence of $\sqrt{3} \times \sqrt{3}$ Mg–Al ordering combined with different stacking sequences (Krivovichev *et al.*, 2010a, 2010b; Zhitova *et al.*, 2010, 2018, 2023a) (Table 1). The $2\sqrt{3} \times 2\sqrt{3}$ (or $\sqrt{12} \times \sqrt{12}$) structure was not determined and refined for any LDH (for almost 30 years after the first report) and was considered questionable. Moreover, the crystal chemical mechanism of potential formation of the $2\sqrt{3} \times 2\sqrt{3}$ superstructure in LDHs remained unclear, as experimental observations have shown that the ordering of di- and trivalent cations (rather common for LDHs) do not result in such long-periodic (within *xy* plane) structures (e.g. Walenta 1984; Bonaccorsi *et al.*, 2007). This attracted our attention to the crystal chemical investigation of charmarite, which is a subject of this work.

Materials

The charmarite studied in this work originates from the Mont Saint-Hilaire alkaline complex. The specimen was collected in 2004 and is in a private collection. The mineral occurs as hexagonal yellowish crystals and curved colourless hexagonal plates up to 0.05 mm in size (Fig. 1), grouped chaotically in clusters that overgrow dark-brown tabular laverovite crystals (1 cm × 1 cm in size) in association with white albite.

Methods

Chemical composition

The chemical analyses (5 points) were carried out with a Hitachi FlexSEM 1000 scanning electron microscope equipped with energy-dispersive spectrometry (EDS) Xplore Contact 30 detector and Oxford AZtecLive STD system of analysis. Analytical conditions were: accelerating voltage 15 kV, beam

https://doi.org/10.1180/mgm.2024.11 Published online by Cambridge University Press

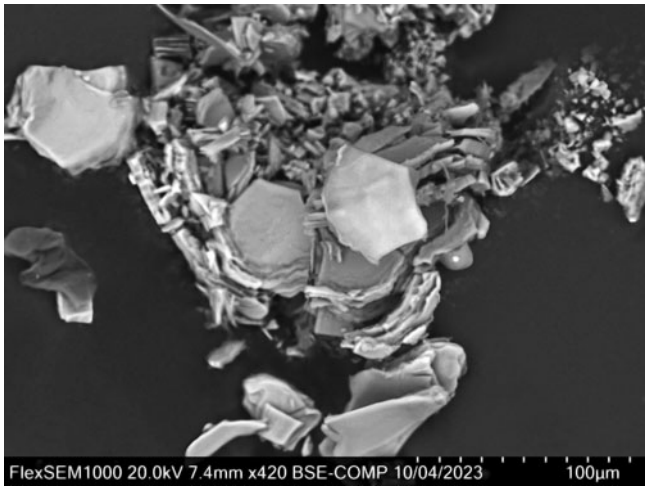

Figure 1. Back-scattered electron image of a bunch of charmarite crystals studied in this work.

current 5 nA and beam size 2 µm. The standards used are given in Table 2.

Single-crystal X-ray diffraction

The single-crystal X-ray diffraction (SCXRD) data have been obtained from tabular hexagonal crystals of reddish colour. The experiment was carried out with Mo*K*α radiation by means of a Bruker Apex II Duo diffractometer (Bruker, Billerica, MA, USA) operated at 50 kV/1 mA and equipped with a charge coupled device (CCD) area detector.

The unit-cell check based on 250 reflections indicated the trigonal symmetry of the mineral (*P* cell) with $a = b = 10.97$ and $c = 15.08$ Å. The full SCXRD data set was collected and separately processed using Bruker and CrysAlis software in automatic and manual (including a check for twin domains) mode. The intensity data were reduced and corrected for Lorentz, polarisation, and background effects using the *CrysAlis PRO* program (CrysAlis PRO, 2014). A semi-empirical absorption-correction based upon the intensities of equivalent reflections was applied (Bruker-AXS, 2014, Sheldrick, 2015). The unit-cell parameters were refined by the least-squares methods. Using *Olex2* (Dolomanov *et al.*, 2009), the structure was solved with the *SHELXS* (Sheldrick, 2008) structure solution program using direct methods and refined with the *SHELXL* (Sheldrick, 2015) refinement package using least squares minimisation. The two-component twinning by matrix {$\bar{1}$ 0 0 / 0 $\bar{1}$ 0 / 0 0 1} was applied to the structure refinement. Crystal structures were visualised using the *Vesta* program (Momma and Izumi, 2011). All procedures resulted in the confirmation of the aforementioned lattice. The topology of the model obtained was reasonable and the search for a higher symmetry using the *Platon* software (Spek, 2003) confirmed the correct choice of the space-group symmetry. Note that we have also obtained structure models in the space groups *P*3, $P\bar{3}m1$ and $P\bar{6}2m$, but none of these provided an improvement over the $P\bar{3}$ model. The alternative refinements in space group $P\bar{3}m1$ resulted in $R_1 = 0.1883$ based on 2222 unique observed reflections and without considerable structural difference and in the space group $P\bar{6}2m$ the refinement converged to $R_1 = 0.0827$ based on 2202 unique observed reflections with non-equivalent interlayers that seemed to us crystal chemically unreasonable.

Table 2. Chemical composition of charmarite.

Constituent	Wt.%	Range	S.D.	Standards
MgO	0.22	0.07–0.40	0.13	Mg_2SiO_4
MnO	46.98	46.69–47.43	0.32	Mn_2SiO_4
FeO	0.15	0.05–0.26	0.09	FeS_2
Al_2O_3	17.19	16.87–17.86	0.39	Kyanite
$CO_2^{(1)}$	7.42			
$H_2O^{(2)}$	27.25			
Total	99.21			

(1)calculated by charge balance;
(2)calculated from the ideal stoichiometry of charmarite.
S.D. – standard deviation

Powder X-ray diffraction

Powder XRD data were collected from an intergrowth of lamellar charmarite crystals up to 0.2 mm in size using a Rigaku R-Axis Rapid II diffractometer (Debye-Scherrer geometry and $d = 127.4$ mm) equipped with a rotating anode X-ray source (Co*K*α and λ = 1.79021 Å) and a curved image plate detector. The data were integrated using the software package *Osc2Tab/SQRay* (Britvin *et al.*, 2017) and processed using the International Centre for Diffraction Data (ICDD) database incorporated into the *PDXL* program (Rigaku, 2018). The *h*, *k* and *l* values were calculated using the software package *VESTA* (Momma and Izumi, 2011) from the crystal structure model of charmarite obtained in this work. The unit-cell parameters of charmarite were refined by the Le Bail method implemented in *Topas* software (Bruker-AXS, 2009) using the starting structural model of charmarite reported therein. The refinement was based on the reflections in the 2θ region from 10 to 80°. The background was modelled by a Chebyshev polynomial approximation of the 12-th order; preferred orientation of the sample along the [002] direction was confirmed during the refinement.

Raman spectroscopy

The Raman spectrum of charmarite was obtained by Horiba Jobin-Yvon LabRam HR800 spectrometer, equipped with a solid-state laser (λ = 532 nm) at 50 mW output power and ~6 mW power at the sample surface for an area of 2 µm × 2 µm. The spectrum was recorded with resolution 2 cm^{-1} at room temperature on the plate used previously for powder XRD data collection that had been placed on a glass slide. The plate had been cleared of paratone oil (used for sample attachment in the powder XRD experiment), but some traces may remain. The spectrum was further processed using *LabSpec* (Horiba) software.

Results

Chemical composition

The chemical composition of charmarite in wt.% is given in Table 2. The empirical formula calculated on the basis of the sum of all metal cations = 6 apfu and OH = 12 apfu is: $(Mn_{3.94}Mg_{0.03}Fe_{0.01})_{\Sigma 3.98}Al_{2.01}(OH)_{12}CO_3 \cdot 3H_2O$. The CO_2 content has been calculated by charge balance. The OH and H_2O content has been calculated from stoichiometry of charmarite.

https://doi.org/10.1180/mgm.2024.11 Published online by Cambridge University Press

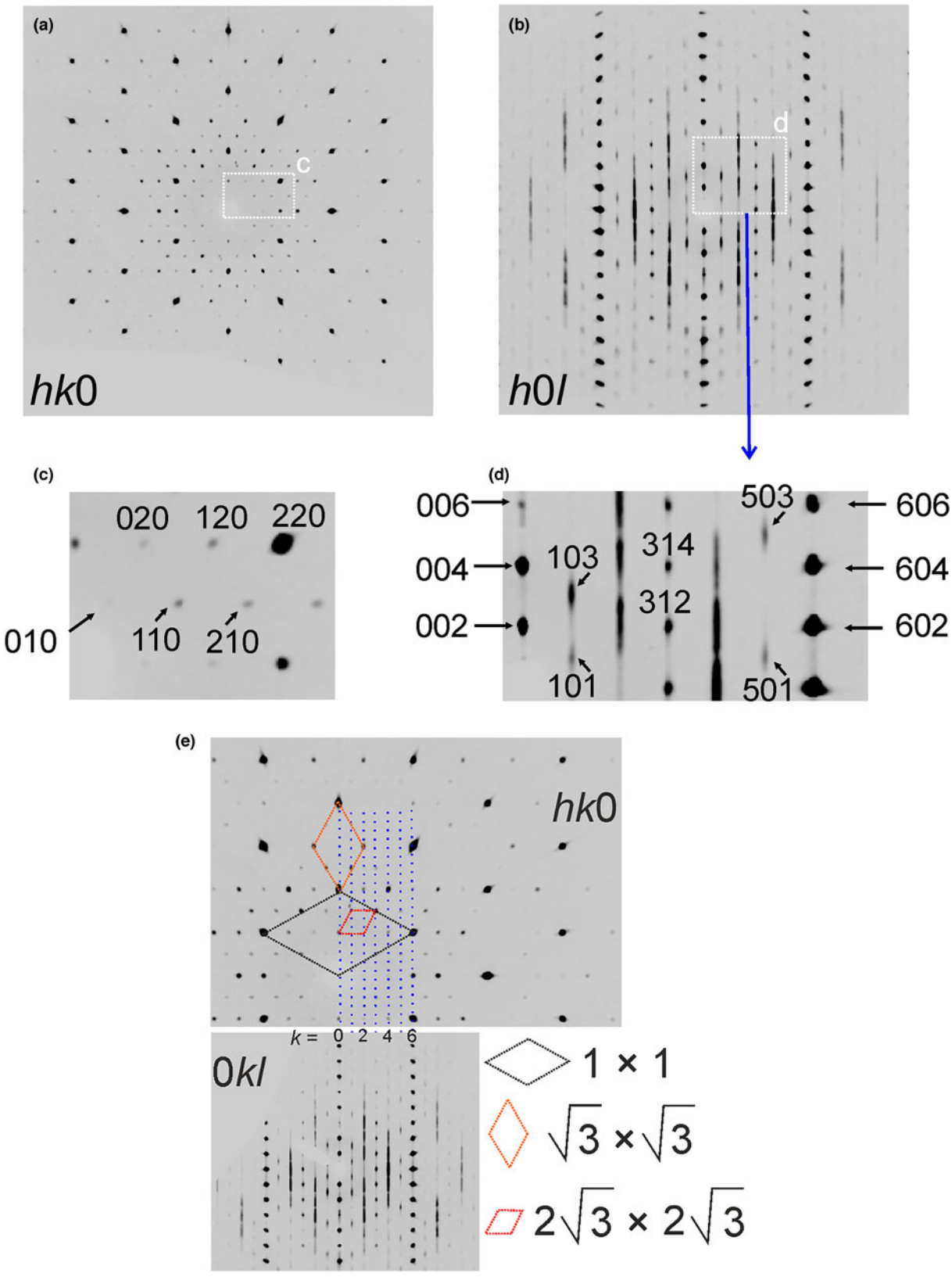

Figure 2. The reciprocal space slices of charmarite: (a) *hk*0 section; (b) *h*0*l* section; (c) enlarged part of *hk*0 section, indexed; (d) enlarged part of *h*0*l* section, indexed; and (e) juxtaposition of *hk*0 and 0*kl* sections.

Single-crystal X-ray diffraction data

The data obtained for charmarite were indexed in the trigonal cell, space group $P\bar{3}$ with the following unit-cell parameters: $a = 10.9630(4)$, $c = 15.0732(5)$ Å and $V = 1568.89(12)$ Å^3. The correct choice of the unit cell is supported by the analysis of the reconstructed reciprocal space slices where regular superstructure reflections are clearly visible (Fig. 2). The crystal structure was

https://doi.org/10.1180/mgm.2024.11 Published online by Cambridge University Press

Table 3. Crystal data, data collection information and structure refinement details for charmarite-2*T*.

Crystal chemical data	
Crystal system	Trigonal
Space group	$P\bar{3}$
a (Å)	10.9630(4)
c (Å)	15. 0732(5)
V (Å^3)	1568.89(12)
Z*	4
Calculated density (g/cm^3)	2.370
Absorption coefficient	3.137
Crystal size, mm	0.1 × 0.1 × 0.05
Data collection	
Diffractometer	Bruker Apex II Duo
Temperature (K)	293(2)
Radiation, wavelength (Å)	Mo*K*α, 0.71073
Range of data collection, 2θ (°)	4.29–75.292
h, *k*, *l* ranges	$-18 \le h \le 17$, $-15 \le k \le 17$, $-25 \le l \le 24$
Total reflection collected	47,865
Unique reflections (R_{int})	5171 (0.0415)
Number of unique reflections $F > 2\sigma(F)$	3801
Data completeness (%)	99.9
Structure refinement	
Refinement method	Full-matrix least-squares on F^2
Weighting coefficients *a*, *b*	0.1766, 2.7007
Data/ restraints/ parameters	5171/13/191
R_1 [$F > 2\sigma(F)$], wR_2 [$F > 2\sigma(F)$]	0.0750, 0.2800
R_1 all, wR_2 all	0.0961, 0.3040
Goodness-of-fit on F^2	1.053
Largest diff. peak and hole (e^- Å^{-3})	1.40/−1.25

* for the formula $Mn_{3.7}Al_{2.3}(OH)_{12}CO_3{\cdot}1.9H_2O$.

solved and refined in the space group $P\bar{3}$ to $R_1 = 0.075$ for 3801 unique observed reflections with $F_o > 2\sigma(F_o)$ (Table 3). Atom coordinates, site occupancies and displacement parameters are given in Table 4. Selected bond lengths and angles are listed in Table 5, the hydrogen bonding scheme is shown in Table 6. The anisotropic displacement parameters are given in Table S1. The crystallographic information file (cif) has been deposited (1) via the joint Cambridge Crystal Data Centre CCDC/FIZ Karlsruhe deposition service; the deposition number is CSD 2285202 and (2) with the Principal Editor of *Mineralogical Magazine* and is available as Supplementary Material (see below).

Juxtaposition of the *hk*0 and 0*kl* reciprocal space sections is shown in Fig. 2e that outlines possible unit cells based on main and superstructure reflections and justifies the choice of lattice with the $2\sqrt{3} \times 2\sqrt{3}$ (or $2\sqrt{3}a$') supercell. The analysis of spots along *l* (stacking direction) shows that (1) a two-layer hexagonal cell is well sustained ($k = 0, 6$); (2) spots with $k = 1$ and 3 are characterised by some diffuse scattering, but are clearly separated and assigned to the $2\sqrt{3} \times 2\sqrt{3}$ ordering along the stacking direction; and (3) the strongest diffuse scattering is observed for the spots with $k = 2$ and 4 that mainly refer to the $\sqrt{3} \times \sqrt{3}$ superstructure. Possibly, the diffuse character of the spots with $k = 2$ and 4 reflects partial Mn–Al disorder in the octahedral sites along the stacking direction (with formation of mixed-occupied positions in some layers) as observed herein.

Powder X-ray diffraction data

Powder XRD data are provided in Table 7, the XRD pattern is presented in Fig. 3. The powder XRD pattern obtained of charmarite is very similar to that from the ICDD card #00-051-1529 (Chao and Gault, 1997), which corresponds to the original description of charmarite-2*H* (crystal structure undetermined, see comparison in Table 7). The polytype notation by Ramsdell (1947) is based on the number of layers within the unit cell and symmetry of the crystal structure. In LDHs there are two main types of layer stacking sequences: hexagonal that normally results in two-layer cells and rhombohedral that normally results in three-layer cells with symmetry reduction from trigonal to monoclinic one-layer cells being also rather widespread (Krivovichev *et al.*, 2010a, 2010b; Zhitova *et al.*, 2018). From powder XRD data and preliminary SCXRD data the layer stacking sequence can be determined: hexagonal or rhombohedral, commonly interpreted as 2*H* and 3*T*/3*R* polytypes, respectively. However, the full symmetry of the crystal structure (e.g. *T*, *H* or *M*) can be affected by cation and/or anion ordering and requires detailed structure analysis. In the original work by Chao and Gault (1997) the polytypes for charmarite, caresite and quintinite were determined as 2*H* and 3*T*. This study shows (by structure refinement using SCXRD data) cation and anion ordering for charmarite with the hexagonal layer stacking sequence resulting in a trigonal cell and polytype notation as 2*T*. The difference in the suffix for polytype notation of 2*T* for charmarite compared to the 2*H* used by Chao and Gault (1997) is not due to any structure differences, but due to structure peculiarities revealed by SCXRD herein. The refined unit-cell parameters of charmarite-2*T* from the powder XRD data are as follows: $a = 10.9934(6)$, $c = 15.1426(11)$ Å and $V = 1584.9(2)$ Å^3.

For the easier comparison of the lattice parameters obtained by different methods we have reduced them to the sublattice, i.e. the distance between the two nearest metal atoms (*a*') and the distance between two octahedral layers (d_{00n}). The obtained values are $a' = a/2/\sqrt{3} = 3.17$ Å obtained by powder XRD *versus* 3.16 Å obtained by single-crystal X-ray diffraction and $d_{00n} = c/2 = 7.57$ Å obtained by powder X-ray diffraction *versus* 7.54 Å obtained by single-crystal X-ray diffraction. The comparison shows that isomorphic substitution (influencing the in-plane *a*' parameter) is negligible. The difference in the *c* parameter (d_{00n}) is larger, but also insignificant for layered compounds and fluctuates around the value of 7.56 Å, which is most often found in stoichiometric quintinite. In view of the insignificance of these changes in d_{00n}, it seems that they may be more likely to be associated with a change in the height of the octahedral layer due distortions of the octahedra, rather than the change in stoichiometry (variations in the M^{2+}:M^{3+} ratio), as the second factor usually causes more significant changes in the interlayer distance, but the height of the octahedral layer fluctuates within 0.0*n* Å (Zhitova *et al.*, 2016). Finally, unit-cell parameters determined by single-crystal and powder X-ray diffraction differ by ~1% (due to multiplication of these small differences), which is a good agreement, taking into account that different crystals of charmarite were studied by these diffraction techniques.

Raman spectroscopy

The Raman spectrum of charmarite-2*T* is shown in Fig. 4a,b and compared with the Raman spectra of quintinite and caresite in Fig. 4 and Table 8. The spectrum contains bands of O–H stretching vibrations and symmetric C–O stretching vibrations that are in agreement with charmarite chemistry in terms of light

https://doi.org/10.1180/mgm.2024.11 Published online by Cambridge University Press

Table 4. Atom coordinates, equivalent isotropic displacement parameters (Å^2), site occupancies and assigned site populations for charmarite-2*T*.

Site	Atom	*x*	*y*	*z*	U_{eq}	s.o.f.	epfu*
Octahedral sheet (type 1)							
*M*1	Mn1	⅔	⅓	0.00966(13)	0.0197(5)	0.62(2)	125(3) e^-,
	Al1	2/3	⅓	0.00966(13)	0.0197(5)	0.38(2)	$Mn_8Al_4(OH)_{24}$
*M*2	Mn2	0.83274(8)	0.16619(8)	0.00148(8)	0.0145(3)	0.76(2)	
	Al2	0.83274(8)	0.16619(8)	0.00148(8)	0.0145(3)	0.24(2)	
*M*3	Mn3	1	0	0	0.0171(7)	0.59(3)	
	Al3	1	0	0	0.0171(7)	0.41(3)	
*M*4	Mn4	½	0	0	0.0115(3)	0.56(2)	
	Al4	½	0	0	0.0115(3)	0.44(2)	
O1	O1	0.6619(4)	0.4971(3)	−0.0643(2)	0.0259(7)	1	
H1	H1	0.664(8)	0.501(8)	−0.1290(13)	0.043	1	
O2	O2	0.6593(4)	0.1577(4)	0.0698(2)	0.0335(8)	1	
H2	H2	0.676(7)	0.192(6)	0.1315(18)	0.043	1	
O3	O3	0.9993(4)	0.1621(4)	−0.06725(19)	0.0287(8)	1	
H3	H3	0.992(8)	0.178(8)	−0.1309(16)	0.043	1	
O4	O4	0.6605(4)	−0.0004(3)	−0.06662(19)	0.0256(7)	1	
H4	H4	0.662(8)	−0.014(7)	−0.1317(15)	0.043	1	
Octahedral sheet (type 2)							
*M*5	Mn5	⅔	⅓	−0.51019(10)	0.0156(3)	0.944(18)	121(3) e^-,
	Al5	⅔	⅓	−0.51019(10)	0.0156(3)	0.056(18)	$(Mn_{7.7}Mg_{0.3})Al_{4.0}(OH)_{24}$
*M*6	Mn6	0.83293(8)	0.16634(8)	−0.50189(5)	0.0122(2)	0.79(2)	
	Al6	0.83293(8)	0.16634(8)	−0.50189(5)	0.0122(2)	0.21(2)	
*M*7	Al7	½	0	−½	0.0128(5)	0.94(2)	
	Mn7	½	0	−½	0.0128(5)	0.06(2)	
*M*8	Al8	1	0	−½	0.0365(18)	0.96(3)	
	Mn8	1	0	−½	0.0365(18)	0.04(3)	
O5	O5	0.8542(3)	0.5023(3)	−0.56955(18)	0.0175(5)	1	
H5	H5	0.846(2)	0.509(2)	−0.6349(8)	0.027	1	
O6	O6	0.6500(3)	0.0013(3)	−0.4342(2)	0.0193(6)	1	
H6	H6	0.679(6)	0.021(6)	−0.3719(16)	0.027	1	
O7	O7	0.5026(3)	0.1524(3)	−0.43631(18)	0.0172(5)	1	
H7	H7	0.500(7)	0.178(6)	−0.3740(18)	0.027	1	
O8	O8	0.9988(3)	0.1473(3)	−0.4338(2)	0.0179(6)	1	
H8	H8	0.998(5)	0.166(5)	−0.3699(13)	0.027	1	
Interlayer gallery							
C1	C1	⅔	⅓	−0.2507(5)	0.0163(14)	0.79(3)	26(1) e^-,
C2	C2	1	0	−0.2502(10)	0.020(2)	0.59(3)	**$C_{2.2(2)}$
C3	C3	⅔	⅓	0.2375(16)	0.028(6)	0.28(3)	
O9	O9	0.7009(6)	0.0344(5)	−0.2540(4)	0.0302(14)	0.67(2)	214(10) e^-,
O10	O10	0.6374(15)	0.0062(11)	−0.2422(9)	0.027(3)	0.273(18)	**$O_{13(2)}$
O11	O11	0.5454(4)	0.2192(4)	−0.2517(3)	0.0309(10)	0.786(15)	
O12	O12	0.9815(5)	0.1063(5)	−0.2540(4)	0.0305(12)	0.588(13)	
O13	O13	0.6472(14)	0.2056(14)	0.2418(11)	0.021(4)	0.172(11)	
O15	O15	0.7321(13)	−0.0027(13)	0.2428(11)	0.044(4)	0.279(15)	
O16	O16	0.6674(5)	0.0668(5)	0.2544(5)	0.0329(15)	0.569(15)	

* epfu – electrons per formula unit; epfu for Mn_8Al_4 (as in ideal formula) is 126 e^-.
**Note: $[(CO_3)(H_2O)_{3.5}]_2$
s.o.f – site occupation factor;

elements (C, H), the determination of which is problematic by other methods. In general, the Raman spectra of charmarite, quintinite and caresite are similar (Table 8), which confirms their structural and chemical similarity.

Discussion

The crystal structure of charmarite consists of two types of metal-hydroxide layers located at the levels $z = 0$ (type 1) and ½ (type 2) and two interlayers located at the levels of $z = ¼$ and ¾ (Fig. 5). Each metal-hydroxide layer consists of four metal sites *M*(1–4) for octahedral sheet 1 and *M*(5–8) for octahedral sheet 2 (Fig. 6). Each *M* site is octahedrally coordinated by OH groups. The $M(OH)_6$ octahedra are edge-shared to form brucite-type sheets.

The octahedral sheets of type 2 are characterised by the contrasting occupancy of the *M* sites: the *M*(5) and *M*(6) sites are nearly fully occupied by Mn, while the *M*(7) and *M*(8) sites are almost completely occupied by Al. This agrees well with the average *M*–O distances and the polyhedral volumes of the respective octahedra: the Mn-occupied octahedra (both *M*(5)- and *M*(6)-centred) have an average *M*(5,6)–O distance of 2.18 Å (and polyhedral volumes of 12.8–12.9 Å^3), while the Al-centred octahedra have <*M*(7)–O> = 1.92 Å and <*M*(8)–O> = 1.90 Å (with polyhedral volumes equal to 9.3 and 9.1 Å^3, respectively). The Mn-centred octahedra exhibit significant angular distortion (Table 9) in order to fit to the lengths of shared edges with neighbouring small $Al(OH)_6$ octahedra (the shared edge of ~2.58 Å) and large $Mn(OH)_6$ octahedra (the shared edge of ~2.99 Å) (Fig. 6c). The geometry of the $Al(OH)_6$ octahedra

https://doi.org/10.1180/mgm.2024.11 Published online by Cambridge University Press

Table 5. Selected bond distances (in Å) for charmarite-2*T*.

Octahedral sheet 1			
*M*1–O2	2.092(4) ×3	*M*2–O2	2.123(4)
*M*1–O1	2.136(3) ×3	*M*2–O1	2.118(3)
<*M*1–O>	2.114	*M*2–O4	2.123(3)
		*M*2–O4	2.107(3)
*M*3–O3	2.049(4) ×6	*M*2–O3	2.119(3)
<*M*3–O>	2.049	*M*2–O3	2.103(4)
		<*M*2–O>	2.116
*M*4–O1	2.037(3) ×2		
*M*4–O2	2.031(4) ×2	*M*5–O7	2.201(3) ×3
*M*4–O4	2.028(3) ×2	*M*5–O5	2.156(3) ×3
<*M*4–O>	2.032	<*M*5–O>	2.178
*M*6–O7	2.178(3)	*M*7–O7	1.915(3) ×2
*M*6–O6	2.170(3)	*M*7–O6	1.914(3) ×2
*M*6–O6	2.168(3)	*M*7–O5	1.922(3) ×2
*M*6–O5	2.177(3)	<*M*7–O>	1.917
*M*6–O8	2.175(3)		
*M*6–O8	2.187(3)	*M*8–O8	1.905(3) ×6
<*M*6–O>	2.176	<*M*8–O>	1.905
Interlayer gallery			
C1–O11	1.292(3) ×3	C3–O13	1.309(13) ×3
C2–O12	1.280(5) ×3		

seems to be unaffected by distortion (Table 9). The total occupancy of the *M*(5–8) sites agrees with charmarite ideal stoichiometry Mn_2Al with a small amount of a lighter cation, possibly Mg (total electrons per formula unit = 121(3) e^-, while the ratio Mn:Al = 2:1 suggesting the ideal epfu value of 126 e^-; see Table 5).

The octahedral sheets of type 1 are characterised by the mixed occupancy of the *M*(1–4) sites: the *M*(1) and *M*(2) sites have higher numbers of electrons per formula unit (epfu) in comparison to the *M*(3) and *M*(4) sites. The occupancies agree well with the average *M*–O bond lengths: 2.12 Å for the *M*(1)- and *M*(2)-centred octahedra, 2.05 Å for the *M*(3)-centred octahedra, and 2.03 Å for the *M*(4)-centred octahedra. The general tendency is that the *M*(1) and *M*(2) octahedra are occupied preferentially by Mn, while the *M*(3) and *M*(4) octahedra are occupied preferentially by Al. The layer topology of the octahedral sheet of type 1 agrees with the topology of the octahedral sheet 2 in the position of Mn- and Al-centred octahedra, whereas occupancies of Mn- and Al-centred octahedra are different. The total occupancy of the *M*(1–4) sites is in agreement with the ideal charmarite stoichiometry Mn_2Al as 125(3) e^- versus ideal value of 126 e^- (Table 5).

The interlayers accommodate carbonate groups and H_2O molecules in-between the octahedral sheets. The $C(2)O_3$ carbonate groups concentrate in the trigonal prism formed by *M*(8) (i.e. Al) sites from the adjacent sheets, whereas the $C(1)O_3$ and $C(3)O_3$ carbonate groups are in the trigonal prisms formed by *M*(1) (Mn) and *M*(5) (Mn) sites from the adjacent sheets (Fig. 6b,d). The interaction between the interlayer $(CO_3)^{2-}$ anions and $(OH)^-$ groups of metal-hydroxide layers is realised through O–H···OCO_2 hydrogen bonds. The H atoms not involved in the bonding between OH groups and $(CO_3)^{2-}$ anions form hydrogen bonds to interlayer H_2O molecules (Fig. 5). Octahedral sheets are linked by weak hydrogen bonding to carbonate groups (O···O ≈ 2.90 Å) and H_2O molecules (O···O ≈ 2.6–2.8 Å). The general tendency in the localisation of $(CO_3)^{2-}$ groups is that they do not occur in the neighbouring trigonal prisms of H atoms (Fig. 6b,d). There is some disorder associated with the carbonate and H_2O molecules in interlayers reflected by partial occupancies of the interlayer C and O sites. There are three C sites in the interlayer (Figs 5, 6), however in accord with charge requirements and taking into account two interlayers per unit cell, only two $(CO_3)^{2-}$ groups are needed per one interlayer (per unit-cell mesh) to compensate the charge leading to some statistical disorder in their localisation. The same is also true about the occupancy of interlayer O atoms, some of which belong to $(CO_3)^{2-}$ groups, whereas the rest belongs to H_2O molecules. The local position of H_2O molecules is sensitive to localisation of the $(CO_3)^{2-}$ group and compensates with spare bond strengths of metal-hydroxide layers.

The observed herein $2\sqrt{3} \times 2\sqrt{3}$ superstructure agrees with the arrangement of symmetrically independent Al sites [i.e. *M*(7) and *M*(8) in one sheet]. However, the differences in the geometry of symmetrically independent Al-occupied sites (measured by bond lengths and polyhedral distortions) is small (Table 9), which indicates that these differences are hardly responsible for the doubling of the *a* unit-cell parameter. The

Table 6. Hydrogen bonding scheme for charmarite-2*T*.

D–H	*d*(D–H)	*d*(H···A)	<DHA	*d*(D···A)	A
O1–H1	0.976(19)	1.94(3)	161(6)	2.876(6)	O11
O2–H2	0.986(19)	1.71(3)	161(6)	2.662(16)	O13
O3–H3	0.984(19)	2.00(4)	146(6)	2.867(7)	O12
		1.93(3)	163(6)	2.881(16)	O15
O4–H4	0.993(19)	1.91(3)	159(6)	2.855(7)	O9
		1.72(3)	157(6)	2.664(13)	O10
O5–H5	0.994(12)	1.936(17)	148.7(19)	2.833(8)	O16
O6–H6	0.981(19)	1.79(2)	170(5)	2.761(6)	O9
		1.99(3)	152(5)	2.899(13)	O10
O7–H7	0.985(19)	1.90(3)	162(6)	2.856(6)	O11
O8–H8	0.984(16)	1.84(3)	150(3)	2.738(7)	O12

Table 7. Powder X-ray diffraction data obtained for charmarite-2*T* compared to the original data for charmarite-2*H* provided by Chao and Gault (1997)*.

Charmarite-2*T*, this work							Charmarite-2*H*, Chao and Gault (1997)	
d_{obs} (Å)	d_{calc} (Å)	I_{obs} (%)	I_{calc} (%)	*h*	*k*	*l*	d_{meas} (Å)	I_{rel} (%)
7.56	**7.54**	**100**	**100**	**0**	**0**	**2**	**7.53**	**100**
3.782	**3.768**	**34**	**19**	**0**	**0**	**4**	**3.768**	**60**
2.747	2.741	14	5	2	2	0	2.743	10
2.702	2.696	9	3	2	2	1	2.702	10
	2.696		3	2	2	$\bar{1}$		
2.580	**2.576**	**20**	**9**	**2**	**2**	**2**	**2.578**	**50**
	2.576		**9**	**2**	**2**	$\bar{2}$		
2.409	2.406	12	3	2	2	3	2.410	10
	2.406		3	2	2	$\bar{3}$		
2.222	**2.216**	**21**	**8**	**2**	**2**	**4**	**2.221**	**40**
	2.216		**8**	**2**	**2**	$\bar{4}$		
2.034	2.028	8	2	2	2	5	2.031	10
	2.028		2	2	2	$\bar{5}$		
1.857	**1.852**	**23**	**7**	**2**	**2**	**6**	**1.856**	**40**
	1.852		**7**	**2**	**2**	$\bar{6}$		
1.587	1.582	7	7	6	0	0	1.585	20
1.557	1.553	10	3	2	2	8	1.552	40
	1.553		3	2	2	$\bar{8}$		
1.373	1.370	3	1	4	4	0	1.325	5
1.000	0.999	6	1	2	8	4	n.p.	n.p.
	0.999		1	2	8	$\bar{4}$	n.p.	n.p.
	0.999		1	8	2	4	n.p.	n.p.
	0.999		1	8	2	$\bar{4}$	n.p.	n.p.

* Charmarite-2*H*, ICDD # 00-051-1529; n.p. – not provided by Chao and Gault (1997). The five strongest reflections are highlighted in bold type.

https://doi.org/10.1180/mgm.2024.11 Published online by Cambridge University Press

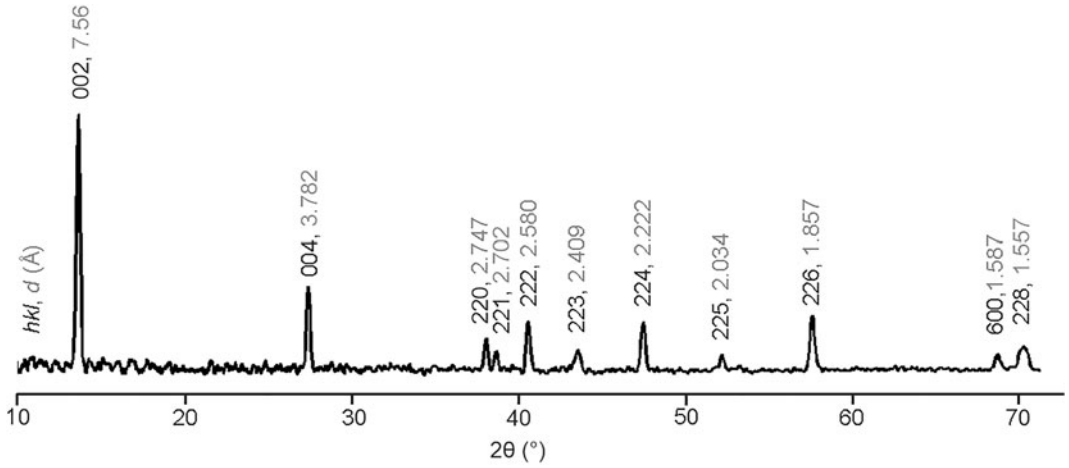

Figure 3. The powder XRD pattern for charmarite.

position of the interlayer components is more remarkable. The analysis of the localisation of the $(CO_3)^{2-}$ anions shows that they are arranged according to the 2×2 superstructure (in which each second trigonal prism is empty) (Fig. 6b,d). At the same time Mn and Al atoms are arranged according to the $\sqrt{3} \times \sqrt{3}$ superstructure. The combination of these superstructures leads to the formation of the $2\sqrt{3} \times 2\sqrt{3}$ superstructure that allows ordering of both (1) Mn and Al cations in octahedral

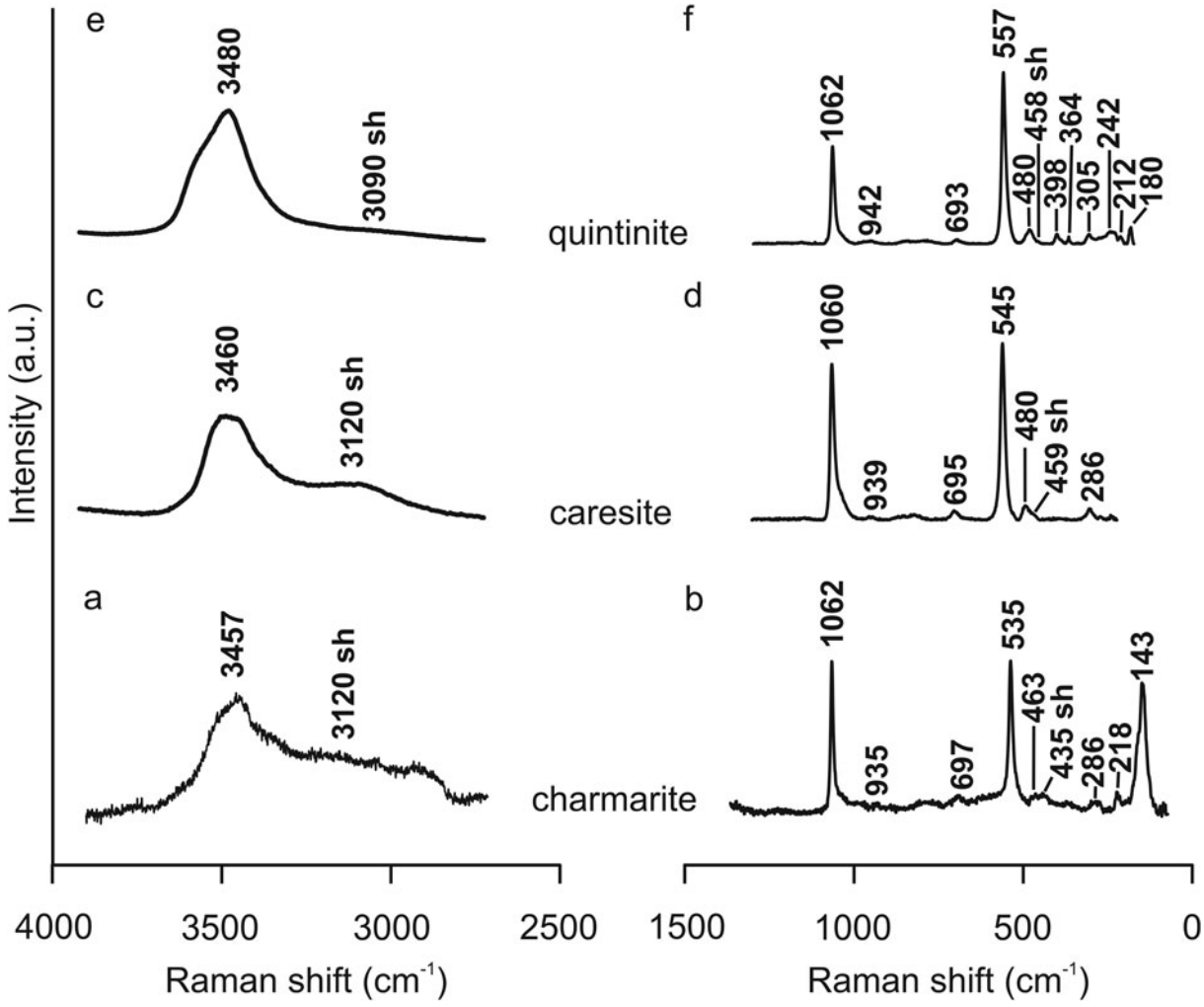

Figure 4. Raman spectrum of charmarite obtained therein: (a) 4000–2500 cm^{-1} range and (b) 1500–0 cm^{-1} range compared to Raman spectra of caresite available in the RRUFF database (under ID: R120028): (c) 4000–2500 cm^{-1} range and (d) 1500–0 cm^{-1} range and quintinite (e,f).

https://doi.org/10.1180/mgm.2024.11 Published online by Cambridge University Press

Table 8. Raman bands observed in the spectra of charmarite, caresite and quintinite and their assignments.

Band assignment	Charmarite	Caresite	Quintinite
O–H stretching vibrations	3457	3460	3485
	3120 sh	3120 sh	3334, 3078
Symmetrical stretching vibrations of carbonate groups	1062	1060	1062, 1046 sh
Water librational modes	935 w	939 w	973 w
Bending mode of carbonate	697 w	695 w	698
Lattice modes, possibly M^{2+}–O–M^{2+} vibrations	535	545	559
Lattice modes	463 w	480 w	484 w
Lattice modes, possibly *M*···O stretching vibrations	435 sh w	459 sh w	401, 367
Lattice modes	286 w	286 w	308
Lattice modes	218 w	-	-
Lattice modes	143	-	-
Reference	This work	*RRUFF database ID: R120028	Theiss *et al.* (2015)

* https://rruff.info/Caresite, accessed on 15 July 2023, Lafuente *et al.* (2015).
sh – shoulder; w – weak

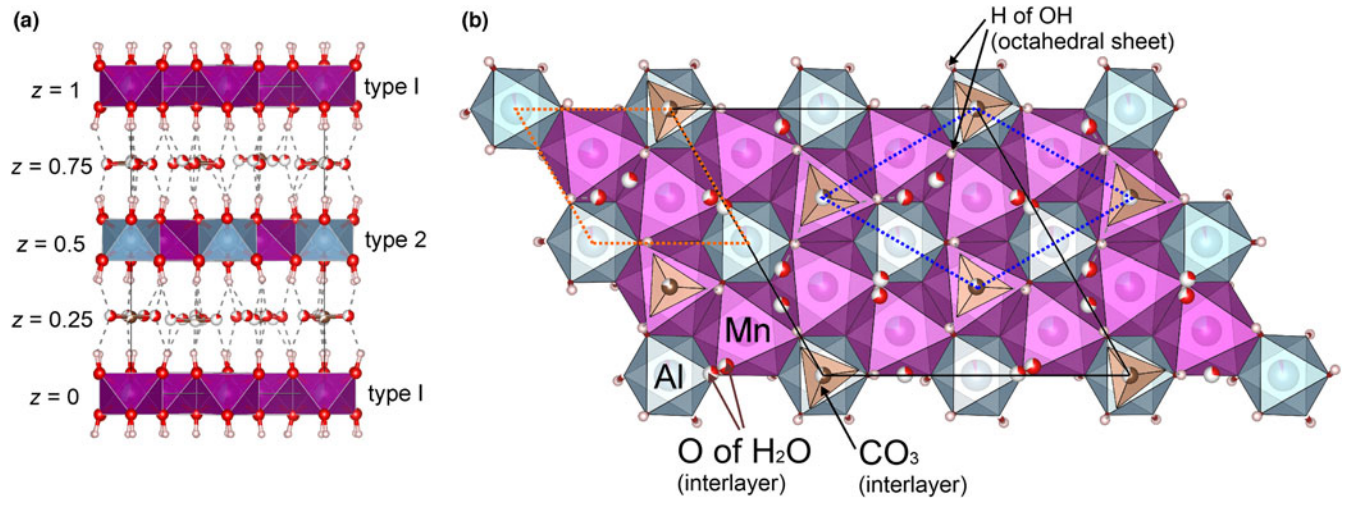

Figure 5. The crystal structure of charmarite-2*T*: (a) projected perpendicular to the stacking direction and (b) within the *xy* plane showing superstructure meshes [the unit cell is outlined by a solid black line; the 2 × 2 superstructure of interlayer carbonate groups ($z = 0.75$) is shown by a blue dashed line; the $\sqrt{3} \times \sqrt{3}$ superstructure of M^{2+} and M^{3+} cations within the octahedral sheet ($z = 0.5$) is outlined by an orange dashed line] (see explanations in the text). Crystal structures were visualised using the *Vesta* program (Momma and Izumi, 2011).

sheets and (2) $(CO_3)^{2-}$ anions in the interlayers. The answer to the question then on why the $2\sqrt{3} \times 2\sqrt{3}$ superstructure has not been previously observed in carbonate and other LDHs may lie in the specific chemical composition of the mineral. According to the data on ionic radii (Shannon, 1976), a six-coordinated Mn^{2+} cation has the radius of 0.81 Å (low spin) or 0.97 Å (high spin). In the crystal structure of charmarite, the *M*(5) site is occupied nearly exclusively by Mn with the *M*(5)–O distance of 2.18 Å. Taking into account the O^{2-} radius of 1.22 Å (Shannon, 1976), the *M*(5)–O distance corresponds to the ionic radius of the high-spin Mn^{2+} ion (0.97 Å). The ionic radius of Al^{3+} is 0.675 Å, while Mg (dominant divalent cation

Table 9. Some geometrical parameters for MO_6 octahedra and occupancies of *M* sites.

Octahedra	<*M*–O> (Å)	Site occupancy	Quadratic elongation	Bond angle variance, degree^2	Distortion index	Polyhedral volume (Å^3)
*M*1	2.114	$Mn_{0.62}Al_{0.38}$	1.03	99	0.010	12.03
*M*2	2.116	$Mn_{0.76}Al_{0.24}$	1.03	93	0.003	12.07
*M*3	2.049	$Mn_{0.59}Al_{0.41}$	1.02	64	0	11.14
*M*4	2.032	$Mn_{0.56}Al_{0.44}$	1.02	61	0.001	10.87
*M*5	2.178	$Mn_{0.94}Al_{0.06}$	1.05	148	0.010	12.86
*M*6	2.176	$Mn_{0.79}Al_{0.21}$	1.05	147	0.002	12.82
*M*7	1.917	$Al_{0.94}Mn_{0.06}$	1.01	30	0.002	9.27
*M*8	1.905	$Al_{0.96}Mn_{0.04}$	1.01	28	0	9.09

Quadratic elongation, bond angle variance, distortion index and polyhedral volume were introduced by Robinson *et al.* (1971) and have been calculated using *Vesta* software (Momma and Izumi, 2011).

https://doi.org/10.1180/mgm.2024.11 Published online by Cambridge University Press

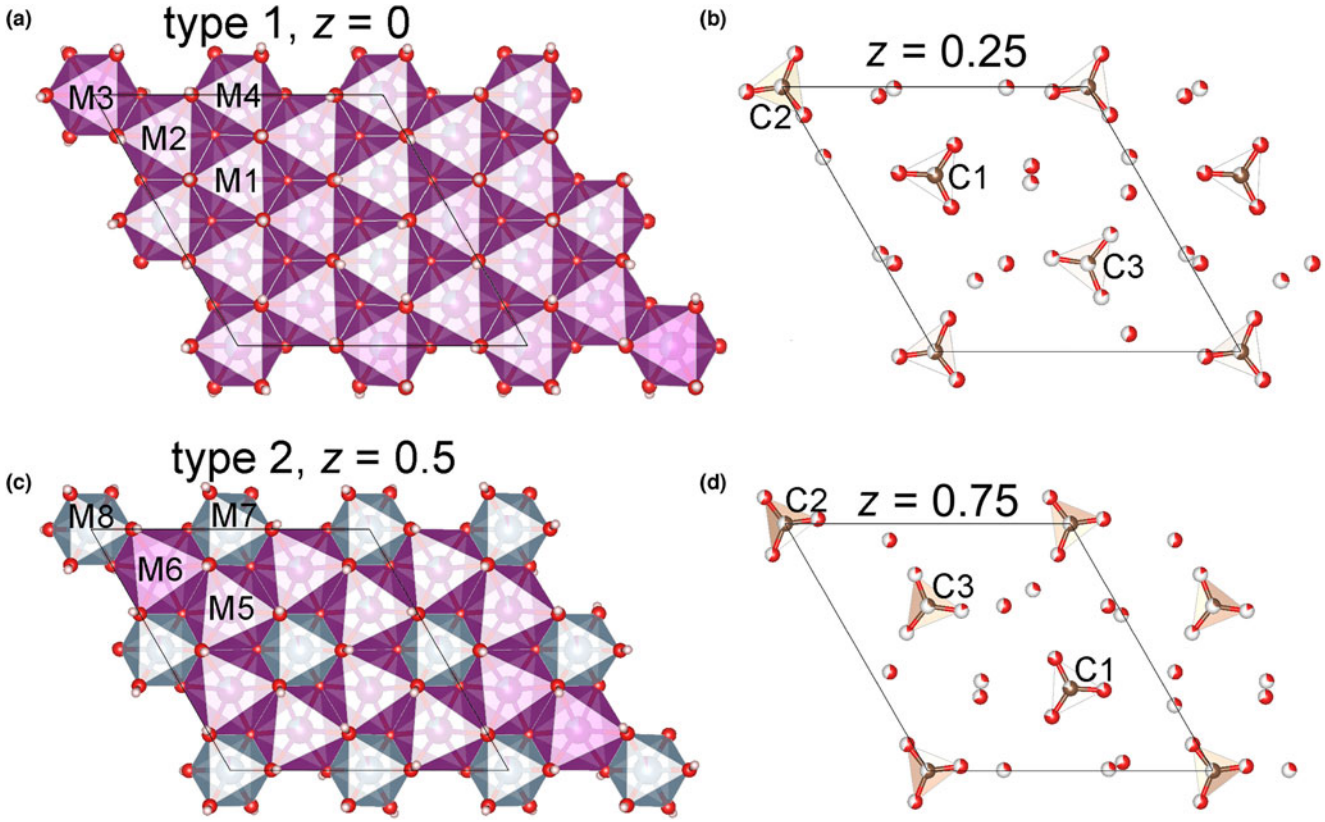

Figure 6. The crystal structure of charmarite-2*T*: (a) octahedral sheet type 1; (b) interlayer at $z = ¼$; (c) octahedral sheet type 2; and (d) interlayer at $z = ¾$. Crystal structures were visualised using the *Vesta* program (Momma and Izumi, 2011).

in quintinite) has the crystal radius of 0.86 Å. So, the species-forming cations Mn^{2+} and Al in charmarite have a more significant difference in the size than Mg and Al in quintinite. Hypothetically, this should lead to the higher tendency of Mn and Al to order as di- and trivalent cations. The higher degree of ordering of di- and trivalent cations within octahedral sheets is responsible for the ordering of interlayer components that follows the scheme of charge distribution. The general tendency revealed recently for Cl-dominant LDHs shows that a higher degree of ordering of di- and trivalent cations leads to the higher degree of ordering of interlayer components, which has been reflected by the occupancy of interlayer Cl and O (of H_2O) sites in chlormagaluminite and dritsite with the $\sqrt{3} \times \sqrt{3}$ superstructure *versus* iowaite that shows the 1×1 (disordered) unit cell (Zhitova *et al.*, 2019b, 2019c; 2023b).

Perhaps, a role may be played by the possibility of detecting weak superstructure reflections and superstructures, which is influenced by factors such as the scattering power of atoms (which is more than twice higher for Mn than for Mg), the crystal quality, and the detector sensitivity. The previous studies of quintinite and chlormagaluminite (Zhitova *et al.*, 2018, 2019b) were performed on the same diffractometer as the one used for the study of charmarite. Therefore, we believe that, among the listed factors, technical reasons are the least likely cause of differences.

Acknowledgements. This research was supported by the Russian Science Foundation (project no. 22-77-10036 for ESZ, AAZ and RMS). Technical support of the St. Petersburg State University Resource Centres "X-ray diffraction research methods" and "Geomodel" is carried out within the framework of SPbSU, grants No. AAAA-A19-119091190094 and No. 116234388, for both Resource Centres, respectively. We would like to thank the reviewers for constructive comments.

Supplementary material. The supplementary material for this article can be found at https://doi.org/10.1180/mgm.2024.11.

Competing interests. The authors declare none.

References

Andersen A.B.A., Henriksen C., Wang Q., Ravnsbæk D.B., Hansen L.P. and Nielsen U.G. (2021) Synthesis and thermal degradation of $MAl_4(OH)_{12}SO_4{\cdot}3H_2O$ with $M = Co^{2+}$, Ni^{2+}, Cu^{2+}, and Zn^{2+}. *Inorganic Chemistry*, **60**, 16700–16712.

Arakcheeva A.V., Pushcharovskii D.Y., Rastsvetaeva R.K., Atencio D. and Lubman G.U. (1996) Crystal structure and comparative crystal chemistry of $Al_2Mg_4(OH)_{12}(CO_3){\cdot}3H_2O$, a new mineral from the hydrotalcite-manasseite group. *Crystallography Reports*, **41**, 972–981.

Bonaccorsi E., Merlino S. and Orlandi P. (2007) Zincalstibite, a new mineral, and cualstibite: crystal chemical and structural relationships. *American Mineralogist*, **92**, 198–203.

Bosa G., Silva C., Brito B., Terzi C., Wypych F. and Nakagaki S. (2023) Revisiting the synthesis of gibbsite, a precursor for Li/Al LDH synthesis and its use as a support for porphyrin immobilization. *Journal of the Brazilian Chemical Society*, **35**, https://doi.org/10.21577/0103-5053.20230095.

Britto S. and Kamath P.V. (2011) Polytypism in the lithium–aluminum layered double hydroxides: The $[LiAl_2(OH)_6]^+$ layer as a structural synthon. *Inorganic Chemistry*, **50**, 5619–5627.

Britvin S.N., Dolivo-Dobrovolsky D.V. and Krzhizhanovskaya M.G. (2017) Software for processing the X-ray powder diffraction data obtained from the curved image plate detector of Rigaku RAXIS Rapid II diffractometer.

Zapiski Rossiiskogo Mineralogicheskogo Obshchestva, **146**, 104–107 [in Russian with English abstract].

Bruker-AXS (2009) *Topas, version 4.2; General Profile and Structure Analysis Software for Powder Diffraction Data*. Bruker-AXS, Karlsruhe, Germany.

Bruker-AXS (2014) *APEX2; Version 2014.11-0*. Bruker AXS, Madison, WI, USA.

Chao G.Y. and Gault R.A. (1997) Quintinite-2H, quintinite-3T, charmarite-2H, charmarite-3T and caresite-3T, a new group of carbonate minerals related to the hydrotalcite–manasseite group. *The Canadian Mineralogist*, **35**, 1541–1549.

CrysAlis PRO (2014) *CrysAlis PRO*. Agilent Technologies Ltd., Yarnton, UK.

Dolomanov O.V., Blake A.J., Champness N.R. and Schröder M. (2009) OLEX: new software for visualization and analysis of extended crystal structures. *Journal of Applied Crystallography*, **36**, 1283–1284.

Evans D.G. and Slade R.C.T. (2005) Structural aspects of layered double hydroxides. Pp. 1–87 in: *Layered Double Hydroxides* (Duan, X. and Evans, D.G. editors). Structure and Bonding, **vol 119**. Springer, Berlin, Heidelberg.

Forano C., Hibino T., Leroux F. and Taviot-Guého C. (2006) Chapter 13.1 layered double hydroxides. *Developments in Clay Science*, **1**, 1021–1095.

Grand L.M., Palmer S.J. and Frost R.L. (2010) Synthesis and thermal stability of hydrotalcites containing manganese. *Journal of Thermal Analysis and Calorimetry*, **100**, 981–985.

Guilherme V.A., Cunha V.R.R., de Paula E., de Araujo D.R. and Constantino V.R.L. (2022) Anti-inflammatory and analgesic evaluation of a phytochemical intercalated into layered double hydroxide. *Pharmaceutics*, **14**, 934.

Karim A.V., Hassani A., Eghbali P. and Nidheesh P.V. (2022) Nanostructured modified layered double hydroxides (LDHs)-based catalysts: a review on synthesis, characterization, and applications in water remediation by advanced oxidation processes. *Current Opinion in Solid State and Materials Science*, **26**, 100965.

Karpenko V.Yu., Zhitova E.S., Pautov L.A., Agakhanov A.A., Siidra O.I., Krzhizhanovskaya M.G., Rassulov V.A. and Bocharov V.N. (2020) Akopovaite, $Li_2Al_4(OH)_{12}(CO_3)(H_2O)_3$, a new Li member of the hydrotalcite supergroup from Turkestan Range, Kyrgyzstan. *Mineralogical Magazine*, **84**, 301–311.

Krivovichev S.V., Yakovenchuk V.N., Zhitova E.S., Zolotarev A.A., Pakhomovsky Y.A. and Ivanyuk G.Yu. (2010a) Crystal chemistry of natural layered double hydroxides. I. Quintinite 2*H*–3*c* from the Kovdor alkaline massif, Kola peninsula, Russia. *Mineralogical Magazine*, **74**, 821–832.

Krivovichev S.V., Yakovenchuk V.N., Zhitova E.S., Zolotarev A.A., Pakhomovsky Y.A. and Ivanyuk G.Yu. (2010b) Crystal chemistry of natural layered double hydroxides. 2. Quintinite–1*M*: first evidence of a monoclinic polytype in M^{2+}-M^{3+} layered double hydroxides. *Mineralogical Magazine*, **74**, 833–840.

Krivovichev S.V., Antonov A.A., Zhitova E.S., Zolotarev A.A., Krivovichev V.G. and Yakovenchuk V.N. (2012) Quintinite-1M from the Bazhenov deposit (Middle Urals, Russia): crystal structure and properties. *Bulletin of St. Petersburg University*. Series 7: Geology, Geography, **2**, 3–10 [in Russian with English abstract].

Lafuente B., Downs R.T., Yang H. and Stone N. (2015) The power of databases: the RRUFF project. Pp. 1–30 in: *Highlights in Mineralogical Crystallography* (T. Armbruster and R.M. Danisi, editors). W. De Gruyter, Berlin, Germany.

Mills S.J., Christy A.G., Génin J.-M.R., Kameda T. and Colombo F. (2012) Nomenclature of the hydrotalcite supergroup: natural layered double hydroxides. *Mineralogical Magazine*, **76**, 1289–1336.

Mills S.J., Christy A.G. and Schmitt R.T. (2016) The creation of neotypes for hydrotalcite. *Mineralogical Magazine*, **80**, 1023–1029.

Momma K. and Izumi F. (2011) VESTA 3 for three-dimensional visualization of crystal, volumetric and morphology data. *Journal of Applied Crystallography*, **44**, 1272–1276.

Ramsdell L.S. (1947) Studies on silicon carbide. *American Mineralogist*, **32**, 64–82.

Rigaku (2018) *PDXL: Integrated X-Ray Powder Diffraction Software, Version 2.8.4.0 (October 23, 2018)*. Tokyo, Japan.

Rives V. (2001) *Layered Double Hydroxides: Present and Future*. Nova Science Publishers: New York, USA.

Robinson K., Gibbs G.V. and Ribbe P.H. (1971) Quadratic elongation: a quantitative measure of distortion in coordination polyhedra. *Science*, **172**, 567–570.

Serna C.J. (1982) Crystal-chemical study of layered $[Al_2Li(OH)_6]^+X^-{\cdot}nH_2O$. *Clays and Clay Minerals*, **30**, 180–184.

Shannon R.D. (1976) Revised effective ionic radii and systematic studies of interatomic distances in halides and chalcogenides. *Acta Crystallographica*, **A32**, 751–767.

Sheldrick G.M. (2008) A short history of SHELX. *Acta Crystallographica*, **A64**, 112–122.

Sheldrick G.M. (2015) Crystal structure refinement with SHELXL. *Acta Crystallographica*, **C71**, 3–8.

Sissoko I., Iyagba E.T., Sahai R. and Biloen P. (1985) Anion intercalation and exchange in $Al(OH)_3$ - derived compounds. *Journal of Solid State Chemistry*, **60**, 283–288.

Sotiles A.R. and Wypych F. (2019) Converting Mn/Al layered double hydroxide anion exchangers into cation exchangers by topotactic reactions using alkali metal sulfate solutions. *Chemical Communications*, **55**, 7824–7827.

Spek A.L.J. (2003) Single-crystal structure validation with the program PLATON. *Journal of Applied Crystallography*, **36**, 7–13.

Theiss F., López A., Frost R.L. and Scholz R. (2015) Spectroscopic characterisation of the LDH mineral quintinite $Mg_4Al_2(OH)_{12}CO_3{\cdot}3H_2O$. *Spectrochimica Acta Part A: Molecular and Biomolecular Spectroscopy*, **150**, 758–764.

Walenta K. (1984) Cualstibit, ein neues Sekundärmineral aus der Grube Clara im mittleren Schwarzwald (BRD). *Chemie der Erde*, **43**, 255–260.

Wang S.L., Liu C.H., Wang M.K., Chuang Y.H. and Chiang P.N. (2009) Arsenate adsorption by Mg/Al–NO_3 layered double hydroxides with varying the Mg/Al ratio. *Applied Clay Science*, **43**, 79–85.

Xu M. and Wei M. (2018) Layered double hydroxide-based catalysts: recent advances in preparation, structure, and applications. *Advanced Functional Materials*, **28**, 1802943.

Zhitova E.S., Yakovenchuk V.N., Krivovichev S. V., Zolotarev A.A., Pakhomovsky Y.A. and Ivanyuk G.Yu. (2010) Crystal chemistry of natural layered double hydroxides. 3. The crystal structure of Mg,Al-disordered quintinite-2*H*. *Mineralogical Magazine*, **74**, 841–848.

Zhitova E.S., Krivovichev S.V., Pekov I.V., Yakovenchuk V.N. and Pakhomovsky Y.A. (2016) Correlation between the *d*-value and the M^{2+}:M^{3+} cation ratio in Mg–Al–CO_3 layered double hydroxides. *Applied Clay Science*, **130**, 2–11.

Zhitova E.S., Popov M.P., Krivovichev S.V., Zaitsev A.N. and Vlasenko N.S. (2017) Quintinite–1*M* from the Mariinsky deposit, Ural Emerald Mines, Central Urals, Russia. *Geology of Ore Deposits*, **59**, 745–751.

Zhitova E.S., Krivovichev S.V., Yakovenchuk V.N., Ivanyuk G.Yu., Pakhomovsky Y.A. and Mikhailova J.A. (2018) Crystal chemistry of natural layered double hydroxides: 4. Crystal structures and evolution of structural complexity of quintinite polytypes from the Kovdor alkaline-ultrabasic massif, Kola peninsula, Russia. *Mineralogical Magazine*, **82**, 329–346.

Zhitova E.S., Krivovichev S.V., Pekov I.V. and Greenwell H.C. (2019a) Crystal chemistry of natural layered double hydroxides. 5. Single-crystal structure refinement of hydrotalcite, $[Mg_6Al_2(OH)_{16}](CO_3)(H_2O)_4$. *Mineralogical Magazine*, **83**, 269–280.

Zhitova E.S., Krivovichev S.V., Pekov I.V. and Yapaskurt V.O. (2019b) Crystal chemistry of chlormagaluminite, $Mg_4Al_2(OH)_{12}Cl_2(H_2O)_2$, a natural layered double hydroxide. *Minerals*, **9**, 221.

Zhitova E.S., Pekov I.V., Chaikovskiy I.I., Chirkova E.P., Yapaskurt V.O., Bychkova, Y.V., Belakovsky D.I., Chukanov N.V., Zubkova N.V., Krivovichev S.V. and Bocharov, V. N. (2019c) Dritsite, $Li_2Al_4(OH)_{12}Cl_2{\cdot}3H_2O$, a new gibbsite-based hydrotalcite supergroup mineral. *Minerals*, **9**, 492.

Zhitova E.S., Sheveleva R.M., Zolotarev A.A. and Krivovichev S.V. (2023a) The crystal structure of Mg–Al–CO_3 layered double hydroxide. *Crystals*, **13**, 839.

Zhitova E.S., Chukanov N.V., Pekov I.V., Zolotarev A.A., Shilovskikh V.V. and Bocharov V.N. (2023b) Crystal chemistry of iowaite, $Mg_6Fe^{III}_2(OH)_{16}Cl_2{\times}4H_2O$, a natural layered double hydroxide. *Applied Clay Science*, **243**, 107070.

https://doi.org/10.1180/mgm.2024.11 Published online by Cambridge University Press